

1 **Epoxide as a Precursor to Secondary Organic Aerosol Formation from**
2 **Isoprene Photooxidation in the Presence of Nitrogen Oxides**

3

4 Ying-Hsuan Lin^a, Haofei Zhang^{a,†}, Havalala O. T. Pye^b, Zhenfa Zhang^a, Wendy J. Marth^a, Sarah
5 Park^a, Maiko Arashiro^a, Tianqu Cui^a, Sri Hapsari Budisulistiorini^a, Kenneth G. Sexton^a, William
6 Vizuite^a, Ying Xie^b, Deborah J. Luecken^b, Ivan R. Piletic^b, Edward O. Edney^b, Libero J.
7 Bartolotti^c, Avram Gold^a, Jason D. Surratt^{a,*}

8

9 ^aDepartment of Environmental Sciences and Engineering, Gillings School of Global Public
10 Health, The University of North Carolina at Chapel Hill, Chapel Hill, NC 27599, USA

11

12 ^bNational Exposure Research Laboratory, Office of Research and Development, U.S.
13 Environmental Protection Agency, Research Triangle Park, NC 27711, USA

14

15 ^cDepartment of Chemistry, East Carolina University, Greenville, NC 27858, USA

16

17 [†]Now at Lawrence Berkeley National Laboratory, Berkeley, CA 94720, USA

18

19 *Corresponding Author: Jason D. Surratt, Department of Environmental Sciences and
20 Engineering, Gillings School of Global Public Health, University of North Carolina at Chapel
21 Hill, Chapel Hill, North Carolina 27599, USA. Tel: (919)-966-0470; Email: surratt@unc.edu

22

23 Author contributions: Y.-H.L., H. Z., H.O.T.P., E.O.E., L.J.B., A.G., J.D.S. designed research;
24 Y.-H.L., H.Z., H.O.T.P., Z.Z., W.J.M., S.P., M.A., T.C., S.H.B., K.G.S., Y.X., D.J.L., I.R.P.,
25 E.O.E., L.J.B., A.G., J.D.S. performed research; Y.-H.L., H.Z., H.O.T.P., Z.Z., W.V., D.J.L.,
26 I.R.P., E.O.E., L.J.B., A.G., J.D.S. analyzed data; Y.-H.L., H.Z., H.O.T.P., E.O.E., L.J.B., A.G.,
27 and J.D.S. wrote paper.

28

29

30 The authors declare no conflict of interest.

31

32 For Submission To: Proceedings of the National Academy of Sciences (PNAS) USA

33 Classification: PHYSICAL SCIENCES (major area): Environmental Sciences (minor area)

34 Manuscript Information: Number of Text Pages – 23 (includes references and figure legends);
35 Number of Figures – 5

36

37

38 **Abstract**

39 Isoprene is a substantial contributor to the global secondary organic aerosol (SOA) burden, with
40 implications for public health and the climate system. The mechanism by which isoprene-derived
41 SOA is formed and the influence of environmental conditions, however, remain unclear. We
42 present evidence from controlled smog chamber experiments and field measurements that in the
43 presence of high levels of nitrogen oxides ($\text{NO}_x = \text{NO} + \text{NO}_2$) typical of urban atmospheres, 2-
44 methyloxirane-2-carboxylic acid (methacrylic acid epoxide; MAE) is a precursor to known
45 isoprene-derived SOA tracers, and ultimately to SOA. We propose that MAE arises from
46 decomposition of the OH adduct of methacryloylperoxynitrate (HOMPAN). This hypothesis is
47 supported by the similarity of SOA constituents derived from MAE to those from photooxidation
48 of isoprene, methacrolein, and MPAN under high- NO_x conditions. Strong support is further
49 derived from computational chemistry calculations and Community Multiscale Air Quality
50 (CMAQ) model simulations, yielding predictions consistent with field observations. Field
51 measurements taken in Chapel Hill, NC, considered along with the modeling results indicate the
52 atmospheric significance and relevance of MAE chemistry across the U.S., especially in urban
53 areas heavily impacted by isoprene emissions. Identification of MAE implies a major role of
54 atmospheric epoxides in forming SOA from isoprene photooxidation. Updating current
55 atmospheric modeling frameworks with MAE chemistry could improve the way that SOA has
56 been attributed to isoprene based on ambient tracer measurements, and lead to SOA
57 parameterizations that better capture the dependency of yield on NO_x .

58

59

60

61 \body

62 **Introduction**

63 Isoprene (2-methyl-1,3-butadiene, C₅H₈) is released by terrestrial vegetation in an estimated
64 quantity of 600 Tg-yr⁻¹ (1) and represents the largest single non-methane hydrocarbon emission
65 into Earth's atmosphere. Photooxidation of isoprene by hydroxyl radicals (OH) during the
66 daytime (2) has been identified as a source of tropospheric ozone (O₃) (3) and secondary organic
67 aerosol (SOA) (4-11). Recent work has shown that anthropogenic pollutants, particularly
68 mixtures of nitrogen oxides (NO_x = NO + NO₂) and sulfur dioxide (SO₂), greatly enhance
69 isoprene as a source of SOA (5, 6, 8, 10, 11). While isoprene is thought to be a substantial
70 contributor to global SOA (12, 13), the mechanism by which isoprene-derived SOA is formed
71 and the influence of environmental conditions on SOA formation remain unclear, but are critical
72 to developing PM_{2.5} control strategies for protection of public health and to assessing the impact
73 on the climate system. Community Multiscale Air Quality (CMAQ) model simulations indicate
74 that removal of controllable anthropogenic emissions could affect a reduction of greater than
75 50% in biogenic SOA in the eastern U.S. (14).

76 NO_x-dependent chemical pathways have been proposed to explain isoprene-derived SOA
77 tracers common to both laboratory-generated and organic aerosols in atmospheres typical of the
78 urban environment (15). SOA formation from isoprene under high-NO_x conditions has been
79 ascribed to the oxidation of methacryloylperoxynitrate (MPAN) (10, 16), which laboratory
80 studies have established as a second-generation oxidation product of isoprene (17, 18). High
81 NO₂/NO ratios favor formation of MPAN from both isoprene and methacrolein (MACR)
82 photooxidation and result in enhanced SOA yields (10, 16). Identification of similar chemical
83 constituents in SOA produced from the photooxidation of isoprene, MACR, and MPAN further

84 supports the central role of MPAN oxidation under these conditions (10). Mass spectrometric
85 analysis of oligoesters and their mono nitrated and sulfated derivatives from SOA generated in
86 the high NO₂/NO chamber experiments yields a series of product ions separated by 102 Da,
87 suggesting a common monomeric unit. While a mechanism of oligoester formation remains to be
88 determined, the observation of a common monomeric unit is in accord with a critical single gas-
89 phase intermediate from MPAN photooxidation as an oligoester precursor (10).

90 The mechanism proposed in Fig. 1 for SOA formation from the photooxidation of isoprene in
91 the presence of NO_x shows the published route to MPAN via the H-abstraction channel of the
92 branching reaction of MACR with OH (17-19). The fate of the transient resulting from the
93 addition of OH to MPAN, however, has until recently been a matter of conjecture. Kjaergaard et
94 al. (20) have reported a computational study suggesting that the HOMPAN transient adduct
95 reacts by elimination of nitrate radical (NO₃) followed by an intramolecular rearrangement to
96 hydroxymethylmethyl- α -lactone (HMML), which is suggested as the precursor of known high-
97 NO_x SOA compounds and oligoesters. In Fig. 1 we suggest a second parallel,
98 thermodynamically feasible pathway via rearrangement of HOMPAN to methacrylic acid
99 epoxide (MAE), which yields known high-NO_x SOA marker compounds and oligoesters similar
100 to those previously reported from photooxidation of isoprene, MACR, and MPAN (10, 16, 21).
101 This study presents experimental evidence supported by computational and modeling studies that
102 the most likely route for isoprene-derived SOA under high-NO_x conditions is via the gas-phase
103 intramolecular rearrangement of the HOMPAN adduct to MAE followed by reactive uptake. We
104 have detected gaseous MAE in the local environment, and modeling of MAE production on a
105 local scale is in accord with measured concentrations. Chemical transport modeling of ambient
106 concentrations of gaseous MAE on a large scale over the southeastern U.S. demonstrates a

107 potentially significant contribution of MAE to SOA in regions where isoprene emissions interact
108 with anthropogenic pollutants. Taken together, the results present a coherent picture that strongly
109 supports MAE as a critical intermediate leading to SOA formation from isoprene photooxidation
110 in the presence of NO_x and fills in an important step in the pathway to SOA under conditions
111 where biogenic and anthropogenic emissions interact.

112 **Results and Discussion**

113 **MAE from the Photooxidation of MACR in Presence of NO_x.** The photooxidation of MACR
114 to MAE is confirmed by controlled outdoor smog chamber experiments conducted under the
115 irradiation of natural sunlight at ambient temperature in the presence of NO_x. Initial
116 concentrations of MACR (1 ppmv), NO (400 ppbv) and NO₂ (200 ppbv) were set for
117 optimization of MPAN formation and generation of sufficient oxidation products for off-line
118 chemical analysis based on simulations from a one-dimensional box model (see *SI Text*). Gas-
119 phase samples were collected hourly with two fritted glass bubblers connected in series and
120 preceded by a Teflon filter to remove aerosol. Ethyl acetate was selected as an aprotic collection
121 solvent to avoid the possibility of MAE hydrolysis and the collection train was cooled in an ice
122 bath to minimize the evaporation of solvent and volatile products. The bubbler samples were
123 analyzed by ultra performance liquid chromatography interfaced to a high-resolution quadrupole
124 time-of-flight mass spectrometer equipped with an electrospray ionization source (UPLC/ESI-
125 HR-Q-TOFMS) operated in the negative ion mode. The extracted ion chromatograms (EICs) at
126 the nominal mass of the MAE anion, m/z 101, are compared in Fig. 2. The EIC in Fig. 2A is from
127 a MACR/NO_x photooxidation experiment and in Fig. 2B from an authentic MAE standard in
128 ethyl acetate, which both show a single major peak with an identical retention time. The accurate

129 mass of the extracted ion at m/z 101 corresponds to the composition of the MAE anion
130 ($C_4H_5O_3^-$) within ± 1 mDa for both the bubbler sample and the MAE standard.

131 The quantitative time profile of MAE formation during the course of an MACR
132 photooxidation experiment (Fig. S1) shows that the increase in gaseous MAE tracks with particle
133 nucleation and growth. Since no seed aerosol was introduced into the chamber prior to the
134 experiment, the increase of aerosol mass concentration can be ascribed to nucleation of MAE
135 followed by heterogeneous oxirane ring-opening reactions. Off-line UPLC/ESI-HR-Q-TOFMS
136 analysis of the nucleated aerosol collected on the Teflon filter preceding the tandem bubblers is
137 in accord with this contention. The collected material is comprised primarily of higher order
138 oligoesters with MAE as a common monomeric unit (Table S1), consistent with the high- NO_x
139 MPAN SOA constituents reported in Surratt et al. (10) and high- NO_x MACR SOA constituents
140 reported by other investigators (16, 22), and thus consistent with MAE as the intermediate
141 involved in SOA formation in these experiments.

142 Gas chromatography/flame ionization detection data indicated that complete reaction of
143 MACR was coincident with peak MAE concentration (Fig. S1), and analysis of the back-up
144 bubbler for breakthrough indicated a collection efficiency of 86% for gas-phase MAE. MAE
145 rapidly converts to particle mass and assuming MAE contributes 50–80% of the measured SOA
146 mass in the chamber experiment (8), a range of values for the chamber-based MAE yield was
147 determined. The total MAE mass concentration profile was estimated by summing the mass
148 concentrations of MAE in the particle and gas phases as a function of time for the 50 and 80%
149 contributions. For each total mass contribution, an initial value for the MAE yield was selected
150 and the time profile of the MAE concentration computed using the SAPRC07 chemical
151 mechanism in a one-dimensional box model to obtain the molar yield of MAE. The procedure

152 was repeated, varying the MAE yield until the predicted MAE mass concentration time profile
153 was in agreement with the chamber profile (see Fig. S2). The final MAE yields for the 50 and
154 80% mass contributions provide lower and upper bounds of 0.18 and 0.32, respectively, for the
155 reaction of OH + MPAN to form MAE. See *SI Text* for further details.

156 **Reactive Uptake of MAE onto Acidified Sulfate Aerosol.** The Kleindienst et al. (23) tracer-
157 based source apportionment method uses 2-methylglyceric acid (2-MG) as an isoprene SOA
158 tracer. We are able to provide insight into the mechanism of 2-MG formation by dark reactive
159 uptake of MAE onto preexisting seed aerosols (see Table S2). Fig. S3 demonstrates that the
160 uptake of synthetic MAE onto acidified sulfate aerosols yields substantial SOA mass, while
161 uptake onto preexisting neutral sulfate seed aerosol is negligible. Fig. 3 shows that 2-MG is a
162 component of SOA formed from the reactive uptake of MAE onto pre-existing acidified sulfate
163 aerosol and has also been identified in SOA generated by the photochemical oxidation of both
164 isoprene and MACR in the presence of NO_x, and in PM_{2.5} collected from downtown Atlanta, GA,
165 on August 9, 2008, at an [NO₂]/[NO] ratio of 5.14 (22). Other high-NO_x SOA tracers, such as
166 the sulfate ester of 2-MG (Fig. S4), as well as the 2-MG dimer (24), have also been observed in
167 these systems. The origin of the markers is most readily explained via nucleophilic attack on the
168 oxirane ring of MAE by water to yield 2-MG, SO₄²⁻ to yield 2-MG sulfate, or the carboxylate
169 anion of MAE to yield the 2-MG dimer. Formation of sulfates and oligoesters by acid-catalyzed
170 esterification is kinetically unfavorable under tropospheric conditions (25), and therefore ruled
171 out as a mechanism.

172 SOA yields (mass of SOA formed/initial MAE concentration) from our reactive uptake
173 experiments are not reported because the uptake behavior of MAE is beyond the scope of the
174 thermal equilibrium partitioning approach, and involves competitive kinetics. Additional work is

175 required to obtain the reactive uptake coefficients (or reaction probabilities, γ) to determine the
176 heterogeneous removal rate of MAE. The heterogeneous removal rate will likely be highly
177 variable, depending on particle composition, phase, acidity, presence of surfactants, and liquid
178 water content. Once the heterogeneous removal rate has been determined, the current modeling
179 framework can be refined to represent MAE chemistry in SOA models with increased accuracy.

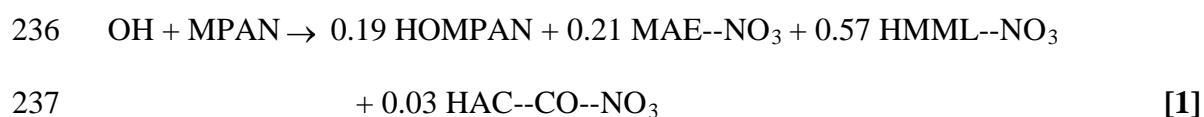
180 **Computational Investigations of the OH + MPAN Reaction Pathway.** As a first step in
181 developing a chemical mechanism for the OH + MPAN addition reaction to form SOA from
182 photooxidation of MACR in the presence of NO_x, calculations were carried out to estimate the
183 total rate constant for this reaction and the yields of its products, including MAE. The energy
184 diagram in Fig. 4 was constructed based on our laboratory and field investigations of the
185 formation of MAE from MACR under high-NO_x conditions and the recent report of Kjaergaard
186 et al. (20) on the potential formation of HMML from OH + MPAN. The quantum chemistry
187 codes GAUSSIAN 2009, NEB, a nudged elastic band approach for identifying minimum energy
188 paths, complexes and transition states, and DIMER for refining transition states and their
189 energies, were used to construct the energy diagram (26-29). All of the quantum chemistry
190 calculations were performed with the m062x density functional in GAUSSIAN 2009, using
191 initially the 6-311++g** orbital basis set.

192 The energy diagram shows the loose and tight transition states, and, as products, the MPAN--
193 OH van der Waals complex, the HOMPAN adduct, and the loosely bound complexes MAE--
194 NO₃, HMML--NO₃, and HAC (hydroxy acetone)--CO--NO₃. The first NEB calculation, carried
195 out between OH + MPAN and HOMPAN revealed a barrierless potential energy curve
196 connecting the loose transition state TS₁, the MPAN--OH van der Waals complex and the tight
197 transition state TS₂. A second NEB calculation between HOMPAN and HAC--CO--NO₃

198 showed HMML--NO₃, along with the tight TS₄ and TS₆ transition states connecting HOMPAN
199 to HMML--NO₃ and HMML--NO₃ to HAC--CO--NO₃, respectively. Since MAE--NO₃ was an
200 expected intermediate in this reaction, a third NEB calculation was set up between HOMPAN,
201 and HAC--CO--NO₃, but this time with MAE--NO₃ as an intermediate in the initial trajectory.
202 The results of this NEB calculation confirmed the presence of MAE--NO₃ and HMML--NO₃ as
203 well as the tight TS₃, TS₅, and TS₆ transition states. The energy minima in Fig. 4 corresponding
204 to OH + MPAN, MPAN--OH, HOMPAN, MAE--NO₃, HMML--NO₃, and HAC--CO--NO₃
205 were refined by computing their structures, energies and vibrational frequencies using the maug-
206 cc-pvtz basis set (30). The same level of theory was employed by DIMER to improve those
207 properties for the tight transition states. The optimized zero point energy-corrected electronic
208 energies, relative to the OH + MPAN energy for MPAN--OH, HOMPAN, MAE--NO₃, HMML--
209 NO₃, HAC--CO--NO₃, and the tight transition states are shown in the diagram.

210 The structures, vibrational frequencies and energies of the reactants and the tight transition
211 states, the fitted Morse parameters for the barrierless potential energy curve, the average energy
212 transfer parameter, and the Lennard–Jones parameters were used as input for VARIFLEX, a
213 widely used chemical kinetics code (31-33), to compute the total rate constant and molar yields
214 for the OH + MPAN reaction at T=300 °K and P=760 Torr. MPAN--OH, HOMPAN, MAE--
215 NO₃, and HMML--NO₃ were subject to both forward and reverse reactions as well as energy-
216 transferring thermalization collisions with the bath gas N₂. Further details concerning the
217 VARIFLEX calculations can be found in the *SI Text*. Using the computed value of -1.80 kcal
218 mol⁻¹ for the TS₂ transition state energy, the total rate constant using VARIFLEX was calculated
219 to be $5.69 \times 10^{-12} \text{ cm}^3 \text{ molecule}^{-1} \text{ s}^{-1}$. This value differs significantly from the experimental value
220 of $3.2 \pm 0.8 \times 10^{-11} \text{ cm}^3 \text{ molecule}^{-1} \text{ s}^{-1}$ at T=275 °K reported by Orlando et al. (18), who noted

221 their measured rate constant was expected to vary little from the value at 300 °K. Recent
222 VARIFLEX calculations of rate constants for OH addition to hydrocarbons containing carbon
223 double bonds have revealed similar differences. Greenwald et al. (34) observed for the OH +
224 ethene addition reaction that decreasing the energy of the transition state analogous to TS₂ by 1.0
225 kcal kmol⁻¹, which is within the expected accuracy of their ab initio calculations, results in good
226 agreement with experimental data between 300 and 400 °K. A similar approach was adopted by
227 Zador et al. (35) in their computational investigations of the OH + propene addition reaction.
228 Consequently, the TS₂ transition state energy in the current study was adjusted to -2.80 kcal mol⁻¹
229 based on the reported improvements in rate constant predictions, and the VARIFLEX
230 calculation was repeated, yielding a rate constant of 3.00 x 10⁻¹¹ cm³ molecules⁻¹sec⁻¹, in good
231 agreement with the experimental value. We note, however (see *SI Text*), that the change in TS₂
232 does not significantly impact the product yields. Using the revised TS₂ transition state energy
233 and neglecting the MPAN--OH van der Waals complex because of its shallow energy minimum
234 and low molar yield coefficient MPAN--OH = -3.10 x 10⁻⁷, our calculations suggest the reaction
235 mechanism, with its molar-based product yields, can be expressed as



238 The VARIFLEX-derived estimate of 0.21 for the yield for MAE is within the range of 0.18–0.32
239 obtained in the chamber-based method. The major pathway for formation of MAE is the addition
240 of OH radical to MPAN forming the chemically activated HOMPAN adduct. NO₃ then leaves
241 HOMPAN by way of the rate determining transition state TS₃, followed by a hydrogen atom
242 transfer and formation of an epoxide (see *Movie S1* for the calculated reaction). HMML warrants
243 discussion as a potentially significant contributor to SOA as a consequence of its molar yield of

244 0.57. As a class, α -lactones are highly labile compounds that have not been observed under
245 conditions relevant to the tropospheric environment (36, 37). Additionally, there are no reports of
246 attempts to generate HMML or to determine its reaction products. 2-Oxooxirane, the
247 unsubstituted structural analog of HMML which would be expected to have similar physico-
248 chemical properties, has been generated in the gas phase at 298 K and 100 Torr with a lifetime of
249 $\sim 150 \mu\text{s}$ (38). The short lifetime of 2-oxooxirane and the data available on α -lactones in general
250 argue against HMML as a major source of SOA. Under atmospheric conditions, thermalized
251 HOMPAN will react with O_2 forming the associated peroxy radical that will undergo further
252 reactions. Additional studies are needed to determine whether these products contribute to SOA
253 formation.

254 **Atmospheric Relevance and Abundance of MAE.** The sampling apparatus used for detection
255 of MAE in the smog chamber photooxidation of MACR was assembled outdoors in Chapel Hill,
256 NC, during summer 2012. The EIC at m/z 101 from UPLC/ESI-HR-Q-TOFMS analysis of the
257 field sample in Fig. 2C shows a peak with a retention time and accurate mass identical to that
258 obtained from the MACR photooxidation under high- NO_x conditions (Fig. 2A) and the MAE
259 standard (Fig 2B). Taken together with the EICs from the chamber studies, the field samples
260 confirm the presence of MAE in the ambient urban atmosphere. The average daytime
261 concentration of $0.34 \mu\text{g m}^{-3}$ ($0.21\text{--}0.75 \mu\text{g m}^{-3}$, $n=6$) and nighttime concentration of $0.16 \mu\text{g m}^{-3}$
262 ($0.07\text{--}0.34 \mu\text{g m}^{-3}$, $n=6$) for gas-phase atmospheric MAE is in accord with expectation for a
263 photochemical oxidation pathway in an area of high isoprene emissions influenced by
264 anthropogenic NO_x , and is strong evidence that MAE is an important intermediate in the high-
265 NO_x photochemistry of isoprene.

266 Fig. S5 shows the diurnal profile of surface layer gaseous MAE from July 21 to August 20,
267 2006 predicted by CMAQ after incorporation of gas-phase MAE chemistry into the model.
268 Concentrations of MAE are predicted to increase in the early morning and peak in the afternoon
269 between 3 and 5 PM local time. The predicted concentrations of MAE vary significantly from
270 day-to-day, with afternoon MAE concentrations ranging from 0.05 to 0.25 $\mu\text{g m}^{-3}$. Noteworthy is
271 the consistency between the CMAQ predicted magnitude and diurnal variation in MAE
272 concentration and field observations from 2012 (Table S2).

273 Fig. 5 shows the estimated concentration of surface layer gaseous MAE over the continental
274 U.S. predicted by CMAQ during one month (July 21 to August 20) in summer 2006 at 12 km by
275 12 km horizontal resolution. The highest MAE concentrations reflect locations with high
276 isoprene emissions, as well as significant anthropogenic activity that can provide NO_x to convert
277 isoprene to MPAN. Near Atlanta, GA, MAE concentrations average around 0.1 $\mu\text{g m}^{-3}$ and can
278 reach up to 0.6 $\mu\text{g m}^{-3}$. Southern California and areas near St. Louis, MO, are also predicted to
279 experience relatively high levels of MAE. In general, concentrations of MAE are predicted to
280 average 0.06 to 0.1 $\mu\text{g m}^{-3}$ across the southeast and near the Ohio River Valley.

281 Uncertainty in predictions of isoprene emissions arise because of local meteorology as well
282 as the modeling algorithm used to parameterize the emission process. CMAQ simulations in this
283 study use BEIS emissions (39), which can be a factor of 2 lower than MEGAN (1) predictions
284 (40). Thus, the gaseous MAE concentrations may be significantly higher than currently displayed
285 in Fig. 5. Furthermore, an aerosol uptake pathway for MAE has not yet been implemented in the
286 model. Uptake to the aerosol phase could extend the lifetime of MAE by suppressing gas-phase
287 reaction with OH. In addition, uncertainty in NO_x predictions as a result of chemistry and
288 emissions, reflected in a high bias in NO_2 for urban areas and low bias in rural areas (41) as well

289 as underestimated NO_3 wet deposition (42) in CMAQ, could lead to differences between
290 measured and observed MAE concentrations.

291 **Atmospheric Implications.** The results presented here strongly support MAE as the precursor of
292 2-MG, the ubiquitous SOA tracer of both isoprene and MACR photooxidation under high- NO_x
293 conditions (10, 15). Reactive uptake of MAE by acidified sulfate seed aerosols and atmospheric
294 aerosols (Fig. 3) points to MAE as the major and heretofore-unidentified precursor to SOA
295 derived from isoprene photooxidation in the presence NO_x . Furthermore, the distribution of the
296 predicted mean gaseous MAE (Fig. 5A) matches the spatial patterns of enhanced summertime
297 aerosol optical thickness over the southeastern U.S. observed by Goldstein et al. (43) (see *SI Text*
298 for spatial distribution of other isoprene-derived high- NO_x products), likely linking our
299 observations with the dominant summertime regional aerosol and the importance of biogenic
300 volatile organic compound-anthropogenic interactions in radiative forcing in climate models.
301 Taken together with the recent detection of isoprene epoxydiols (IEPOX) under low-NO
302 conditions (9-11), identification of MAE also implies epoxides derived from the oxidation of
303 isoprene play a major role as SOA precursors. With respect to MAE, consistency between the
304 predicted and chamber-based values for the yield of MAE as well as between observed ambient
305 MAE levels and the CMAQ predictions are encouraging, and in accord with a contribution of
306 MAE to secondary organic aerosol. However, additional work to develop a robust database of
307 laboratory measurements of the $\text{OH} + \text{MPAN}$ rate constant and product yields is needed to fully
308 evaluate the proposed mechanism. Further investigation of the heterogeneous chemistry of MAE
309 is also needed to elucidate the complex gas-particle interactions necessary to understand the
310 kinetics and chemical fate of MAE under different atmospheric conditions, such as aerosol
311 composition, liquid water content, and aerosol acidity.

312 **Materials and Methods**

313 **MACR/NO_x Photooxidation Experiments.** MACR/NO_x photooxidation experiments were
314 carried out in a fixed volume 120-m³ Teflon film environmental irradiation chamber, located on
315 the roof of the UNC Gillings School of Global Public Health. Initial conditions for each
316 experiment consisted of 1 ppmv MACR, 0.2 ppmv NO, and 0.4 ppmv NO₂. No seed aerosol
317 was injected into the chamber. All reactants were injected into the chamber before sunrise.
318 Measurements from both gas and particle phases were taken periodically until sunset. Detailed
319 operating conditions for chemical and physical monitoring of the chamber have been previously
320 described (44). To detect gaseous MAE formation, chamber air was continuously drawn through
321 two fritted-glass bubblers in series at a sampling flow rate of ~ 1 L min⁻¹. Bubbler samples were
322 collected in ethyl acetate cooled in an ice bath. Teflon membrane filters (Pall Life Science, 47
323 mm diameter, 1.0- μ m pore size) were installed in front of the inlet to the glass bubblers to ensure
324 collection of gas-phase MAE only. Bubbler samples were collected hourly throughout the course
325 of experiments, and analyzed immediately by UPLC/ESI-HR-Q-TOFMS (Agilent 6500 Series)
326 operated in the negative (-) ion mode. 50 μ L aliquots from the bubbler samples were directly
327 injected onto the UPLC/ESI-HR-Q-TOFMS without additional treatment, and quantified with an
328 authentic MAE standard. Details of UPLC/(-)ESI-HR-TOFMS operating conditions and
329 procedures are described elsewhere (21). The detection limit of MAE by UPLC/(-)ESI-HR-
330 TOFMS was 5 pg μ L⁻¹, based on signal-to-noise ratios > 3:1, and the uncertainty was ~3%.

331 **Reactive Uptake Studies Using MAE.** Authentic MAE was synthesized according to
332 procedures described in the *SI Text* and [Fig. S6](#). The synthetic standard was characterized by
333 NMR and UPLC/(-)ESI-HR-Q-TOFMS for confirmation of structure and purity ([Fig. S7-S9](#)).
334 The purity of MAE was determined to be ~ 99%. Reactive uptake of MAE onto preexisting seed

335 aerosols was examined in the UNC 10-m³ flexible Teflon indoor chamber. Details of this
336 chamber have been described previously (11). A scanning electrical mobility sizing (SEMS)
337 system (Brechtel Manufacturing Inc., Hayward, CA) equipped with a cylindrical-geometry
338 differential mobility analyzer (DMA) and a mixing condensation particle counter (MCPC) was
339 used to measure aerosol size distributions. Experiments were conducted with 300 ppbv MAE to
340 ensure collection of sufficient SOA mass for off-line chemical analysis of reaction products.
341 Aerosol samples were collected on Teflon membrane filters (Pall Life Science, 47 mm diameter,
342 1.0- μ m pore size) at a sampling flow rate of $\sim 20 \text{ L min}^{-1}$ for 2 h. For each experiment, two
343 Teflon filters were stacked in the filter holder. Front filters were collected to examine particle-
344 phase reaction products. The back filters served to correct for absorption of gaseous MAE;
345 however, no gaseous MAE was found to absorb. All experiments were carried out under dark
346 and dry conditions ($\text{RH} < 5\%$) at constant temperature (20–25°C). Control experiments,
347 including clean chamber, MAE only, and seed aerosol (acidic and neutral seed) only, were
348 performed to rule out artifacts. Filters collected from these experiments revealed no MAE-
349 derived SOA constituents.

350 **Theoretical Calculations.** All GAUSSIAN 2009, NEB, DIMER and VARIFLEX calculations
351 were run on an IBM iDataPlex cluster with six login nodes, with 160 compute nodes for running
352 batch jobs, located in the National Computer Center on the U.S. EPA campus in Research
353 Triangle Park, North Carolina. Each login node has two quad-core Intel Xeon x5550 processors
354 and 48 GB of memory (6 GB/core), while each compute node has two quad-core Intel Xeon
355 x5550 processors and either 32 GB or 48 GB of memory (4-6 GB/core). The Intel Xeon x5550
356 processors operate at 2.66 GHz. Details of our VARIFLEX calculations are described in the *SI*
357 *Text*.

358 **Ambient Gas and Fine Aerosol Collection and Analyses.** Ambient gas samples were collected
359 in Chapel Hill, NC, during summer 2012. The sampling site was located on the roof of the UNC
360 Gillings School of Global Public Health building. Daytime (09:30-19:30, local time) and
361 nighttime (20:30-06:30, local time) samples were collected. Samples were collected and
362 analyzed in the same manner as gaseous samples collected from outdoor smog chamber studies,
363 and quantified with an authentic MAE standard by UPLC/(-)ESI-HR-TOFMS. Archived
364 ambient fine aerosol samples collected during the summer 2008 Mini-Intensive Gas and Aerosol
365 Study (AMIGAS) in Atlanta, GA, at the Jefferson Street (JST) site were also analyzed. A
366 detailed description of the sampling site and collocated measurements is provided elsewhere (45).
367 Aerosol sample analysis is described in the *SI Text*.

368 **Regional Chemical Transport Model Simulations.** CMAQ Model v5.01 (46, 47) with the
369 SAPRC07 chemical mechanism (48, 49) and isoprene updates (50) was further expanded to
370 explicitly track peroxyacyl radicals from MACR oxidation, isoprene-derived MPAN, and later-
371 generation MPAN oxidation products, including MAE and HMML to estimate ambient
372 concentrations of MAE over the continental U. S. The yields and rate constant for the four
373 MPAN product channels follow the yields estimated through computational chemistry in
374 reaction [1]. See *SI Text* for additional documentation.

375 **ACKNOWLEDGEMENTS.** This research was supported in part by the National Institute of
376 Environmental Health Sciences (P30ES010126). Y.-H.L. and J.D.S. were supported in part by
377 the Electric Power Research Institute (EPRI). Y.-H.L. acknowledges a Dissertation Completion
378 Fellowship from the UNC Graduate School. M.A. and S.H.B. were supported by the National
379 Science Foundation Graduate Research Fellowship Program (NSF-GRFP) and Fulbright
380 Presidential Fellowship Program, respectively. Richard Kamens, Elias Rosen, Glenn Walters,

381 and Denis Fedor are gratefully acknowledged for their assistance in the design and construction
382 of the UNC indoor smog chamber. The authors thank Rodney Weber and Xiaolu Zhang for
383 providing 2008 AMIGAS PM_{2.5} filter samples. The authors also thank Bill Hutzell, Rob Pinder,
384 Jose L. Jimenez, Joel Thornton, Douglas Worsnop, and Manjula Canagaratna for useful
385 discussions. The U. S. Environmental Protection Agency through its Office of Research and
386 Development collaborated in the research described here. It has been subjected to the Agency's
387 administrative review and approved for publication. Mention of trade names or commercial
388 products does not constitute endorsement or recommendation for use.

389 **References**

- 390 1. Guenther A, et al. (2006) Estimates of global terrestrial isoprene emissions using
391 MEGAN (Model of Emissions of Gases and Aerosols from Nature). *Atmos. Chem. Phys.*
392 6(11):3181-3210.
- 393 2. Atkinson R, Arey J (2003) Gas-phase tropospheric chemistry of biogenic volatile organic
394 compounds: A review. *Atmos. Environ.* 37:197-219.
- 395 3. Chameides WL, Lindsay RW, Richardson J, Kiang CS (1988) The role of biogenic
396 hydrocarbons in urban photochemical smog: Atlanta as a case study. *Science*
397 241(4872):1473-1475.
- 398 4. Claeys M, et al. (2004) Formation of secondary organic aerosols through photooxidation
399 of isoprene. *Science* 303(5661):1173-1176.
- 400 5. Edney EO, et al. (2005) Formation of 2-methyl tetrols and 2-methylglyceric acid in
401 secondary organic aerosol from laboratory irradiated isoprene/NO_x/SO₂/air mixtures and
402 their detection in ambient PM_{2.5} samples collected in the eastern United States. *Atmos.*
403 *Environ.* 39(29):5281-5289.

- 404 6. Kroll JH, Ng NL, Murphy SM, Flagan RC, Seinfeld JH (2005) Secondary organic aerosol
405 formation from isoprene photooxidation under high-NO_x conditions. *Geophys. Res. Lett.*
406 32(18):L18808.
- 407 7. Kroll JH, Ng NL, Murphy SM, Flagan RC, Seinfeld JH (2006) Secondary organic aerosol
408 formation from isoprene photooxidation. *Environ. Sci. Technol.* 40(6):1869-1877.
- 409 8. Surratt JD, et al. (2006) Chemical composition of secondary organic aerosol formed from
410 the photooxidation of isoprene. *J. Phys. Chem. A* 110(31):9665-9690.
- 411 9. Paulot F, et al. (2009) Unexpected epoxide formation in the gas-phase photooxidation of
412 isoprene. *Science* 325(5941):730-733.
- 413 10. Surratt JD, et al. (2010) Reactive intermediates revealed in secondary organic aerosol
414 formation from isoprene. *Proc. Natl. Acad. Sci. USA* 107(15):6640-6645.
- 415 11. Lin Y-H, et al. (2012) Isoprene epoxydiols as precursors to secondary organic aerosol
416 formation: Acid-catalyzed reactive uptake studies with authentic compounds. *Environ.*
417 *Sci. Technol.* 46(1):250-258.
- 418 12. Henze DK, Seinfeld JH (2006) Global secondary organic aerosol from isoprene oxidation.
419 *Geophys. Res. Lett.* 33(9):L09812.
- 420 13. Carlton AG, Wiedinmyer C, Kroll JH (2009) A review of Secondary Organic Aerosol
421 (SOA) formation from isoprene. *Atmos. Chem. Phys.* 9(14):4987-5005.
- 422 14. Carlton AG, Pinder RW, Bhave PV, Pouliot GA (2010) To what extent can biogenic
423 SOA be controlled? *Environ. Sci. Technol.* 44(9):3376-3380.
- 424 15. Hallquist M, et al. (2009) The formation, properties and impact of secondary organic
425 aerosol: current and emerging issues. *Atmos. Chem. Phys.* 9(14):5155-5236.

- 426 16. Chan AWH, et al. (2010) Role of aldehyde chemistry and NO_x concentrations in
427 secondary organic aerosol formation. *Atmos. Chem. Phys.* 10(15):7169-7188.
- 428 17. Tuazon EC, Atkinson R (1990) A product study of the gas-phase reaction of
429 Methacrolein with the OH radical in the presence of NO_x. *Int. J. Chem. Kinet.* 22(6):591-
430 602.
- 431 18. Orlando JJ, Tyndall GS, Paulson SE (1999) Mechanism of the OH-initiated oxidation of
432 methacrolein. *Geophys. Res. Lett.* 26(14):2191-2194.
- 433 19. Tuazon EC, Atkinson R (1990) A product study of the gas-phase reaction of Isoprene
434 with the OH radical in the presence of NO_x. *Int. J. Chem. Kinet.* 22(12):1221-1236.
- 435 20. Kjaergaard HG, et al. (2012) Atmospheric Fate of Methacrolein. 2. Formation of Lactone
436 and Implications for Organic Aerosol Production. *J. Phys. Chem. A* 116(24):5763-5768.
- 437 21. Zhang H, Surratt JD, Lin Y-H, Bapat J, Kamens RM (2011) Effect of relative humidity
438 on SOA formation from isoprene/NO photooxidation: enhancement of 2-methylglyceric
439 acid and its corresponding oligoesters under dry conditions. *Atmos. Chem. Phys.*
440 11:6411-6424.
- 441 22. Zhang H, et al. (2012) Secondary organic aerosol formation from methacrolein
442 photooxidation: Roles of NO_x level, relative humidity and aerosol acidity. *Environmental*
443 *Chemistry* 9(3):247-262.
- 444 23. Kleindienst TE, et al. (2007) Estimates of the contributions of biogenic and
445 anthropogenic hydrocarbons to secondary organic aerosol at a southeastern US location.
446 *Atmos. Environ.* 41(37):8288-8300.

- 447 24. Jaoui M, et al. (2008) Formation of secondary organic aerosol from irradiated α -
448 pinene/toluene/NO_x mixtures and the effect of isoprene and sulfur dioxide. *J. Geophys.*
449 *Res.* 113(D9):D09303.
- 450 25. Birdsall AW, Zentner CA, Elrod MJ (2012) Study of the kinetics and equilibria of the
451 oligomerization reactions of 2-methylglyceric acid. *Atmos. Chem. Phys. Discuss.*
452 12:30039-30080.
- 453 26. Frisch MJ, et al. (2009) Gaussian 09 Revision A. 1 (Gaussian Inc., Wallingford CT).
- 454 27. Mills G, Jónsson H, Schenter GK (1995) Reversible work transition state theory:
455 application to dissociative adsorption of hydrogen. *Surf. Sci.* 324(2-3):305-337.
- 456 28. Alfonso DR, Jordan KD (2003) A flexible nudged elastic band program for optimization
457 of minimum energy pathways using ab initio electronic structure methods. *J. Comput.*
458 *Chem.* 24(8):990-996.
- 459 29. Heyden A, Bell AT, Keil FJ (2005) Efficient methods for finding transition states in
460 chemical reactions: Comparison of improved dimer method and partitioned rational
461 function optimization method. *J. Chem. Phys.* 123:224101.
- 462 30. Papajak E, Leverentz HR, Zheng J, Truhlar DG (2009) Efficient Diffuse Basis Sets: cc-
463 pV x Z⁺ and maug-cc-pV x Z. *J. Chem. Theor. Comput.* 5(5):1197-1202.
- 464 31. Klippenstein SJ, Miller JA (2002) From the time-dependent, multiple-well master
465 equation to phenomenological rate coefficients. *J. Phys. Chem. A* 106(40):9267-9277.
- 466 32. Miller JA, Klippenstein SJ (2006) Master equation methods in gas phase chemical
467 kinetics. *J. Phys. Chem. A* 110(36):10528-10544.
- 468 33. Klippenstein SJ, et al. (2008) VARIFLEX, version 2.0 (Argonne National Laboratory,
469 Argonne, IL).

- 470 34. Greenwald EE, North SW, Georgievskii Y, Klippenstein SJ (2005) A two transition state
471 model for radical-molecule reactions: A case study of the addition of OH to C₂H₄. *J.*
472 *Phys. Chem. A* 109(27):6031-6044.
- 473 35. Zádor J, Jasper AW, Miller JA (2009) The reaction between propene and hydroxyl. *Phys.*
474 *Chem. Chem. Phys.* 11(46):11040-11053.
- 475 36. L'abbé G (1980) Heterocyclic analogues of methylenecyclopropanes. *Angew. Chem. Int.*
476 *Ed. Engl.* 19(4):276-289.
- 477 37. Wheland R, Bartlett PD (1970) α -Lactones from diphenylketene and di-*tert*-butylketene.
478 *J. Am. Chem. Soc.* 92(20):6057-6058.
- 479 38. Chen S-Y, Lee Y-P (2010) Transient infrared absorption of *t*-CH₃C(O)OO, *c*-
480 CH₃C(O)OO, and alpha-lactone recorded in gaseous reactions of CH₃CO and O₂. *J.*
481 *Chem. Phys.* 132(11):114303-114311.
- 482 39. Carlton AG, et al. (2010) Model representation of secondary organic aerosol in
483 CMAQv4.7. *Environ. Sci. Technol.* 44(22):8553-8560.
- 484 40. Carlton AG, Baker KR (2011) Photochemical Modeling of the Ozark Isoprene Volcano:
485 MEGAN, BEIS, and Their Impacts on Air Quality Predictions. *Environ. Sci. Technol.*
486 45(10):4438-4445.
- 487 41. Appel KW, et al. (2011) A multi-resolution assessment of the Community Multiscale Air
488 Quality (CMAQ) model v4.7 wet deposition estimates for 2002–2006. *Geosci. Model*
489 *Dev.* 4(2):357-371.
- 490 42. Allen DJ, et al. (2012) Impact of lightning-NO on eastern United States photochemistry
491 during the summer of 2006 as determined using the CMAQ model. *Atmos. Chem. Phys*
492 12:1737-1758.

- 493 43. Goldstein AH, Koven CD, Heald CL, Fung IY (2009) Biogenic carbon and
494 anthropogenic pollutants combine to form a cooling haze over the southeastern United
495 States. *Proc. Natl. Acad. Sci. USA* 106(22):8835–8840.
- 496 44. Ebersviller S, et al. (2012) Gaseous VOCs rapidly modify particulate matter and its
497 biological effects – Part 1: Simple VOCs and model PM. *Atmos. Chem. Phys.* 12:12277-
498 12292.
- 499 45. Hansen DA, et al. (2003) The southeastern aerosol research and characterization study:
500 Part 1-overview. *J. Air Waste Manag. Assoc.* 53(12):1460-1471.
- 501 46. Byun D, Schere KL (2006) Review of the governing equations, computational algorithms,
502 and other components of the models-3 Community Multiscale Air Quality (CMAQ)
503 modeling system. *Appl. Mech. Rev.* 59(1-6):51-77.
- 504 47. Foley KM, et al. (2010) Incremental testing of the Community Multiscale Air Quality
505 (CMAQ) modeling system version 4.7. *Geosci. Model Dev.* 3(1):205-226.
- 506 48. Carter WPL (2010) Development of the SAPRC-07 chemical mechanism. *Atmos.*
507 *Environ.* 44(40):5324-5335.
- 508 49. Hutzell WT, Luecken DJ, Appel KW, Carter WPL (2012) Interpreting predictions from
509 the SAPRC07 mechanism based on regional and continental simulations. *Atmos. Environ.*
510 46(0):417-429.
- 511 50. Xie Y, et al. (2012) Understanding the impact of recent advances in isoprene
512 photooxidation on simulations of regional air quality. *Atmos. Chem. Phys. Discuss.*
513 12(10):27173-27218.

514 **Figure Legends**

515 **Fig. 1.** Proposed mechanism for SOA formation from isoprene photooxidation in the presence of
516 NO_x .

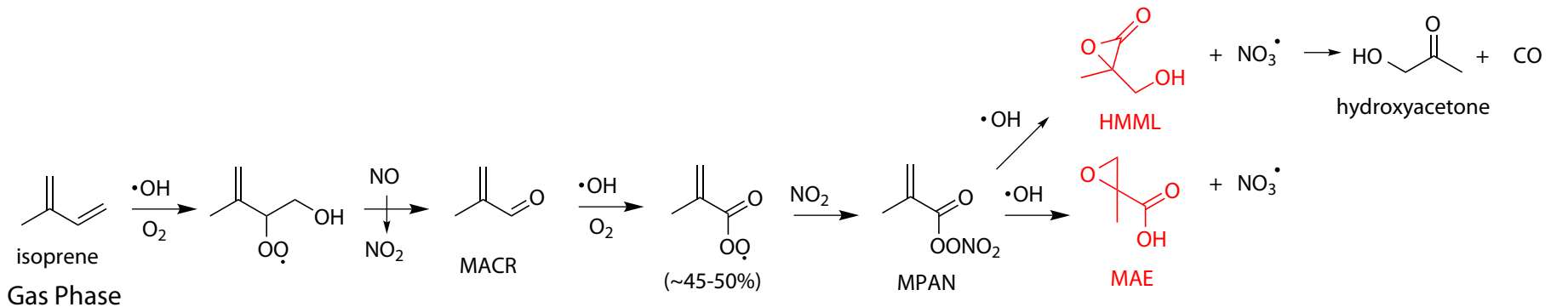
517 **Fig. 2.** Gaseous MAE detected by UPLC/(-)ESI-HR-Q-TOFMS from (A) an irradiated
518 MACR/ NO_x outdoor smog chamber experiment, (B) authentic MAE standard, and (C) an
519 ambient air sample collected in Chapel Hill, NC, during summer 2012.

520 **Fig. 3.** GC/EI-MS traces and corresponding mass spectra showing the presence of 2-MG in
521 aerosol collected from (A) an isoprene/ NO_x photooxidation experiment, (B) an MACR/ NO_x
522 photooxidation experiment, (C) a dark reactive uptake study of MAE, and (D) an ambient $\text{PM}_{2.5}$
523 sample from downtown Atlanta, GA.

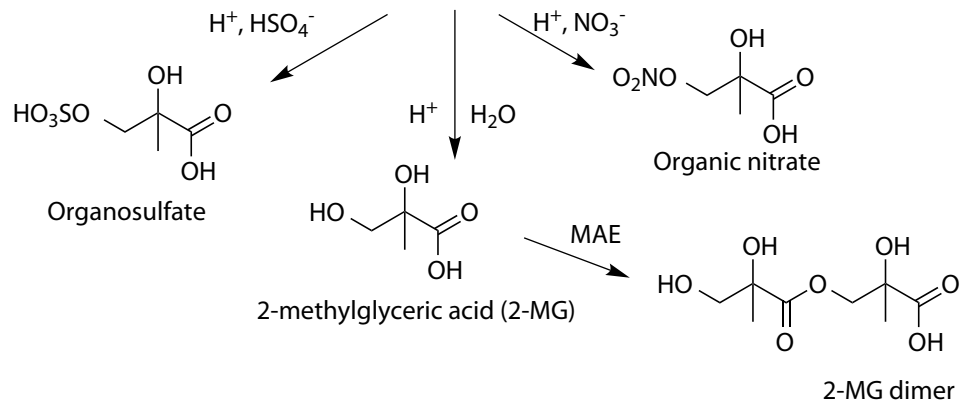
524 **Fig. 4.** Relative ZPE corrected energies (green) and product yields (orange) for the reaction of
525 MPAN with OH calculated at m062x/maug-cc-pvtz level of theory. Results are shown for the
526 adjusted value of $-2.80 \text{ kcal mol}^{-1}$ for the TS_2 transition state energy.

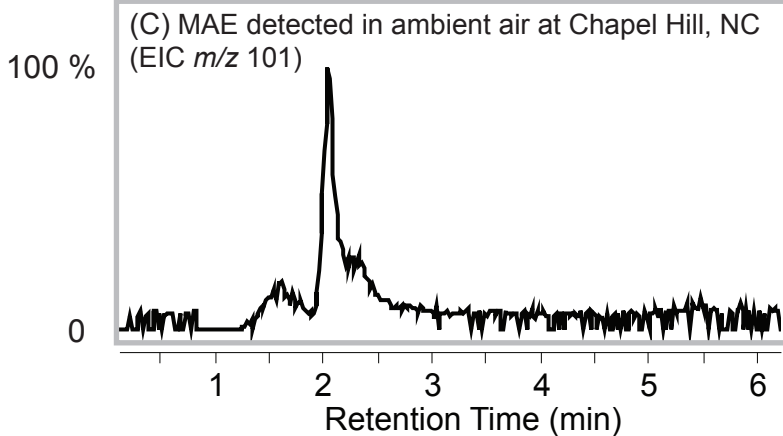
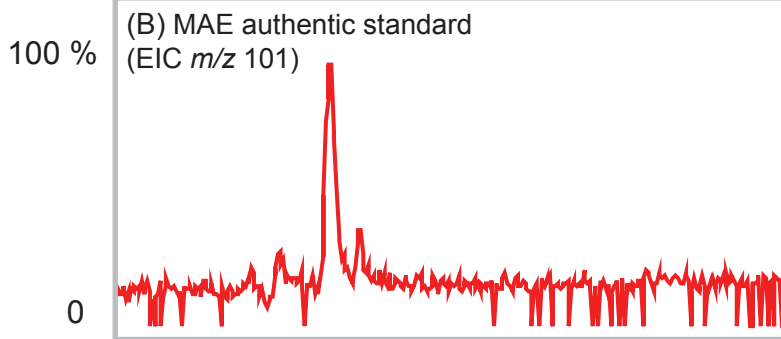
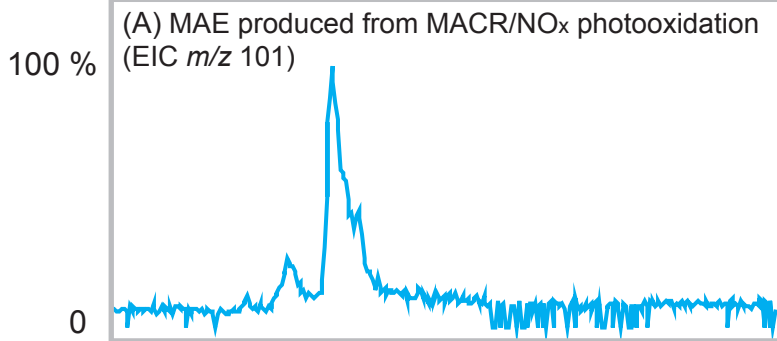
527 **Fig. 5.** July 21 to August 20, 2006 (A) mean and (B) maximum surface layer MAE concentration
528 over the continental U.S. simulated by the updated CMAQ model.

529

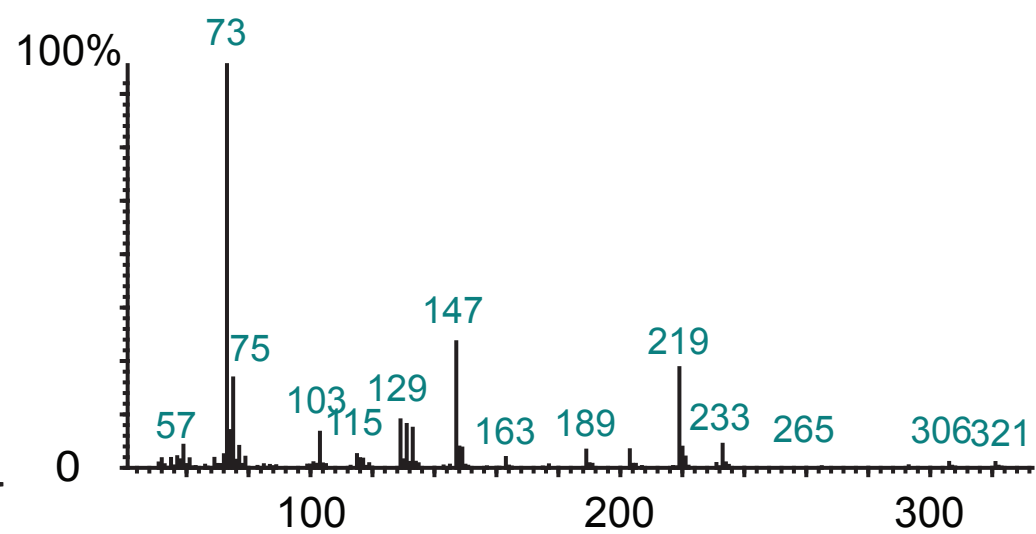
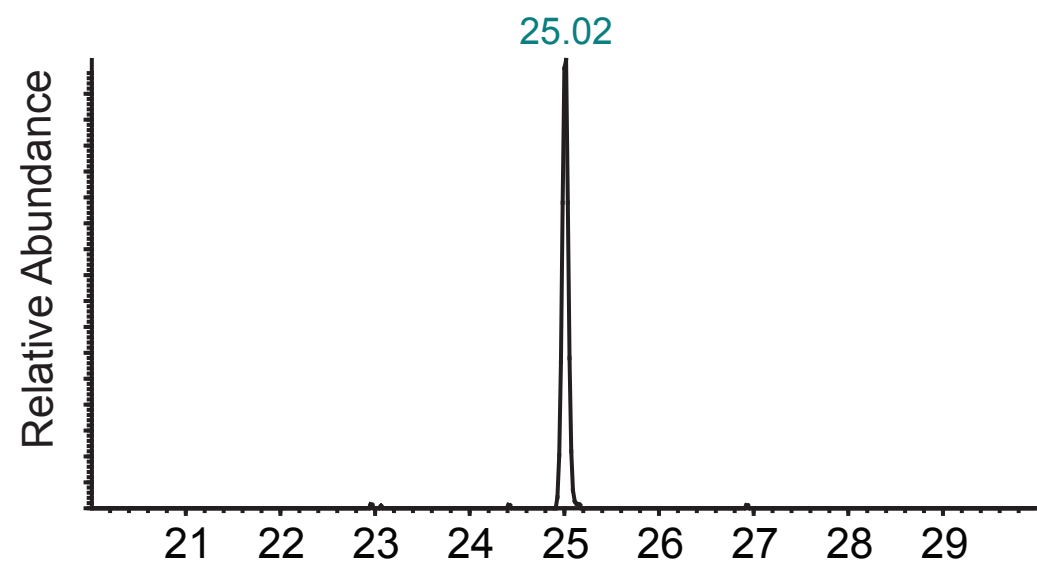


Aerosol Phase

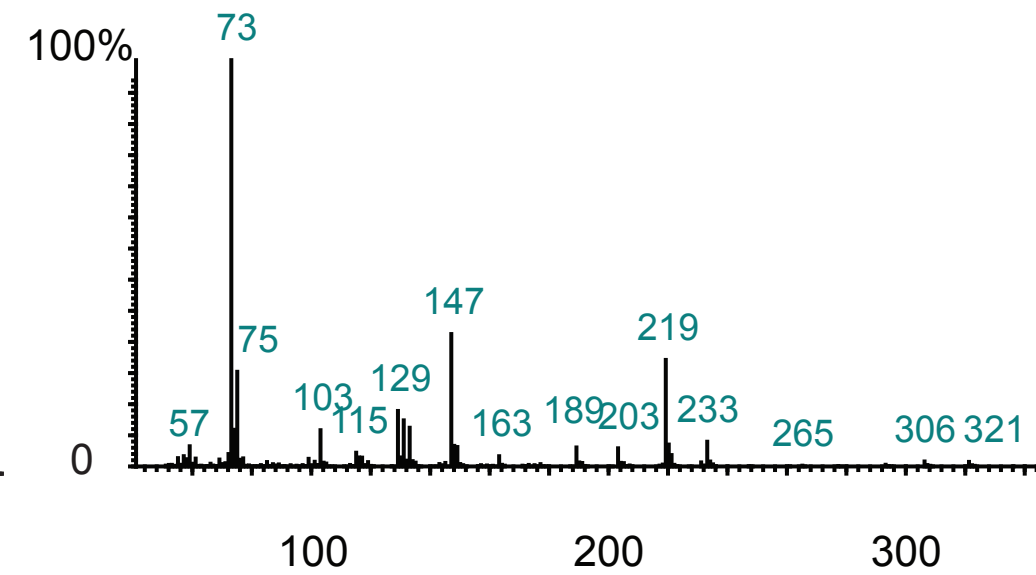
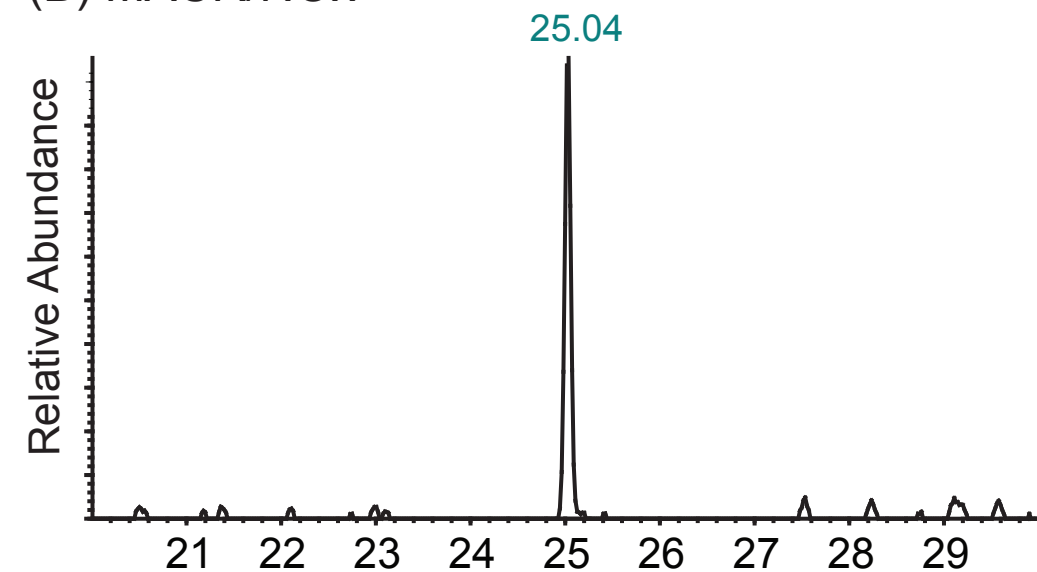




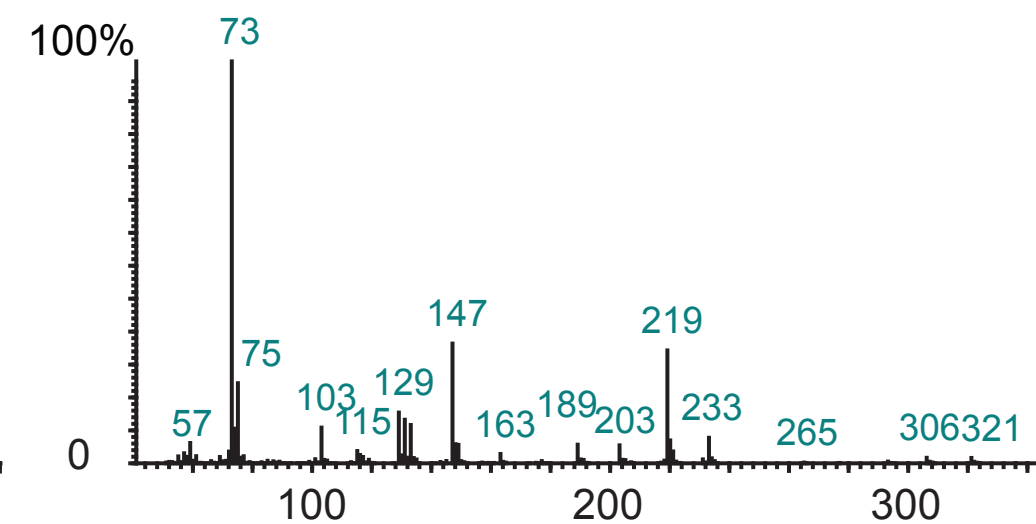
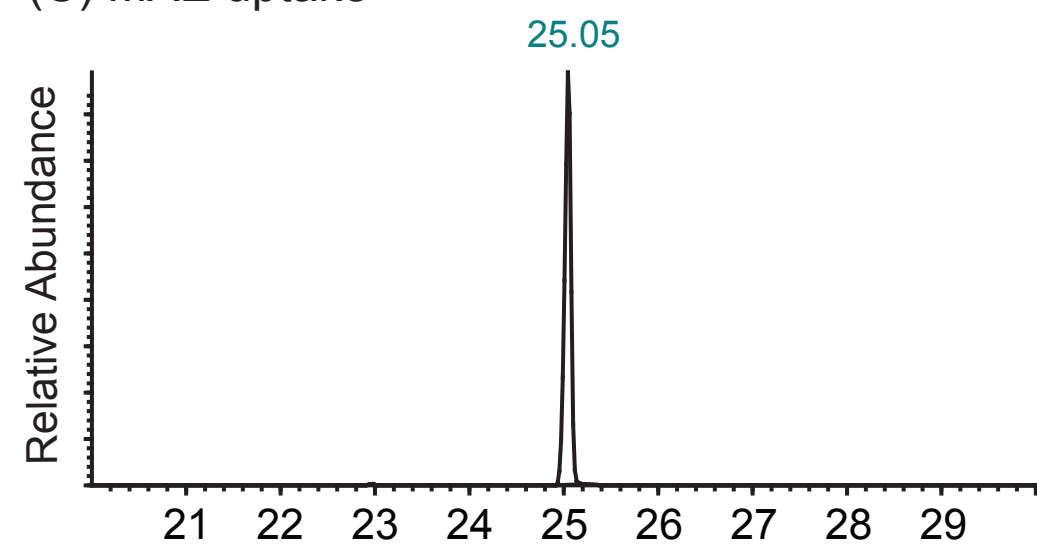
(A) Isoprene/NOx



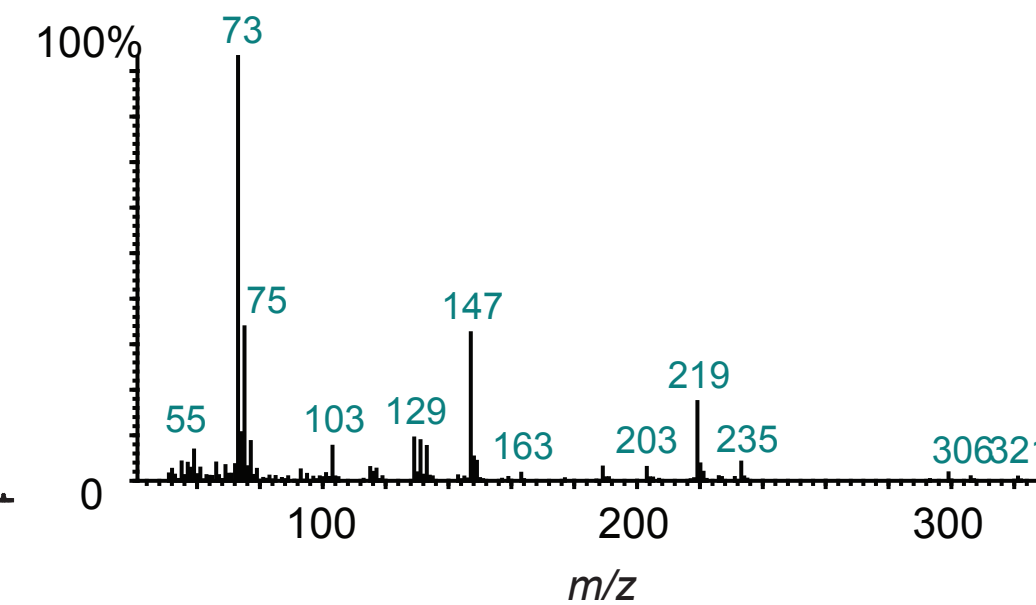
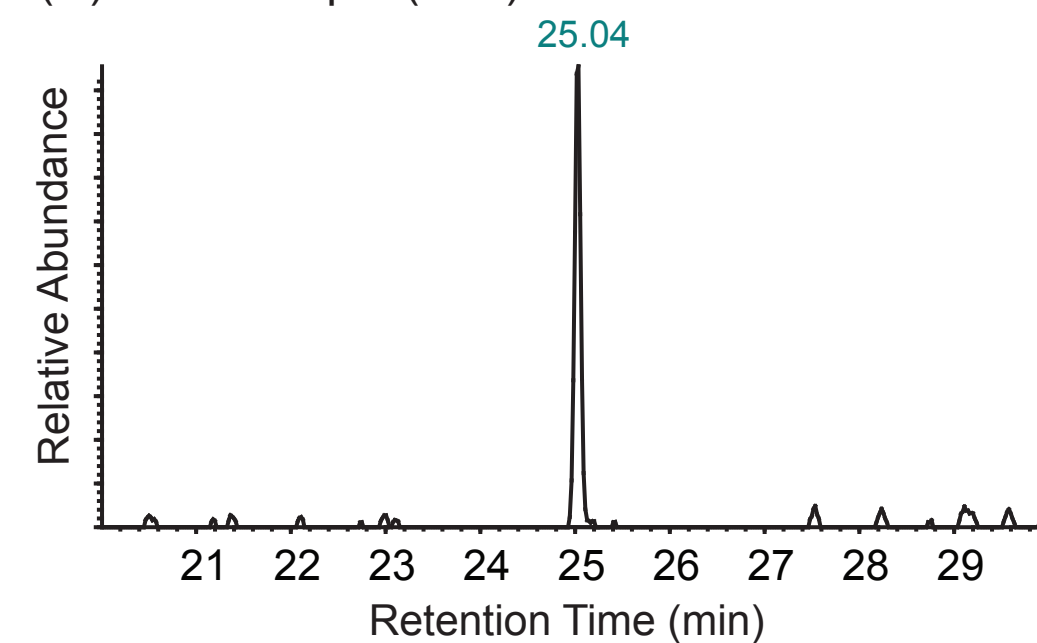
(B) MACR/NOx



(C) MAE uptake

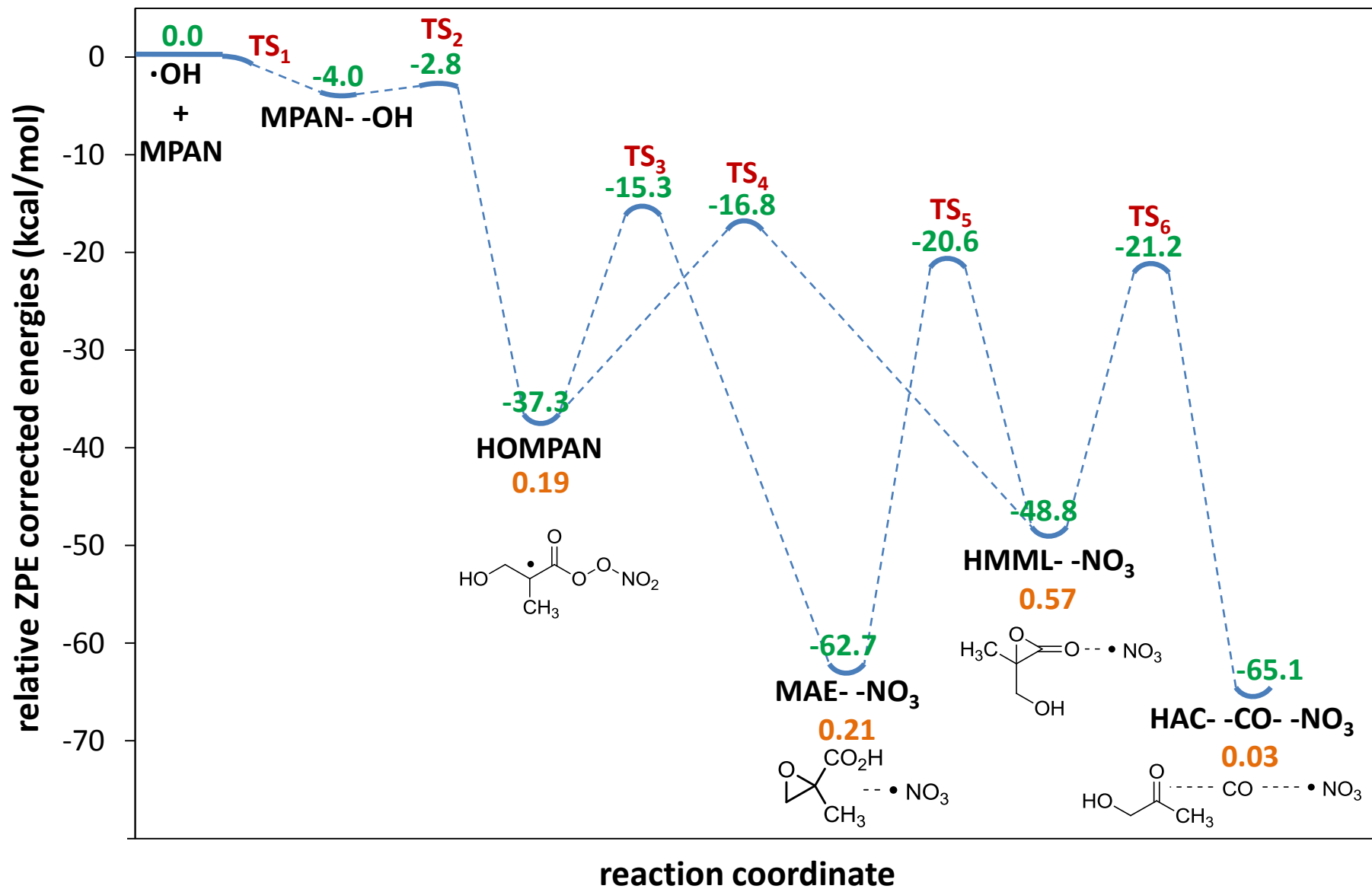


(D) Field sample (JST)



·OH + MPAN

$$k_{\text{total}} = 3.0 \times 10^{-11} \text{ cm}^3 \text{ molecule}^{-1} \text{ s}^{-1} \text{ (T = 300 K, P = 760 Torr)}$$



Predicted MAI ($\mu\text{g m}^{-3}$)

